Acta Cryst. (1992). A48, 737-746

Diffuse Absences due to the Atomic Size Effect

BY B. D. BUTLER, R. L. WITHERS AND T. R. WELBERRY

Research School of Chemistry, Australian National University, GPO Box 4, Canberra City, ACT 2601, Australia

(*Received* 23 *December* 1991; *accepted* 10 *March* 1992)

Abstract

Diffuse intensity absences, on reciprocal planes that pass through the Bragg positions, have been observed in diffraction patterns of $Zr_{0.61}Y_{0.39}O_{1.81}$ and $(Ta_2O_5).7\%(WO_3)$. These absences, occurring on planes normal to near-neighbour directions and highlighted by sheets of diffuse intensity on either side, are shown to result naturally from atomic size effect distortions. The origins of these diffuse features are explained, using both real-space and modulation-wave approaches, by concentrating on a Monte Carlo simulated two-dimensional binary alloy. These absences, which should be characteristic of systems that distort *via* the size effect, result from intensity components that do not depend on scattering-factor differences and so will be most prominent when the atomic species have similar scattering powers, thus suppressing the normal size effect intensity component [Warren, Averbach & Roberts (1951). *J. Appl. Phys.* **22**, 1493-1496].

1. Introduction

The problem of adequately measuring and then correctly interpreting the diffraction patterns of disordered materials has occupied many crystallographers for a very long time (Warren, Averbach & Roberts, 1951; Cowley, 1968; Krivoglaz, 1969; Borie & Sparks, 1971; Hayakawa & Cohen, 1975; Yamamoto & Nakazawa, 1982; Welberry, 1986; Welberry, Withers & Osborn, 1990). Usually, the information most sought after from such studies is the type and extent of atomic ordering on the various sublattices making up the average structure unit cell. Such atomic ordering, or compositional modulation, gives rise to sinusoidal variations of diffuse intensity in reciprocal space, which, if it were possible to measure in isolation, could be back Fourier transformed to yield the desired real-space ordering parameters. The direct extraction of such information from adequately measured diffraction patterns is, however, almost invariably obscured by the fact that atomic ordering (*i.e.* compositional modulation) is always accompanied by some degree of structural relaxation (*i.e.* static atomic displacements) arising from atoms of differing size occupying a single sublattice. The 'atomic size effect' is a term used to describe the additional effects upon the diffraction pattern of such structural relaxation.

In the context of binary substitutionally disordered alloys, a characteristic feature of diffraction patterns due to the atomic size effect was first described by Warren *et al.* (1951). This is the transfer of diffuse intensity from regions on one (*e.g.* the high-angle) side of Bragg peaks to regions on the other (*e.g.* the low-angle) side. More recently, analogous effects have been investigated for molecular crystals (Khanna & Welberry, 1990). Early theories of diffraction from disordered alloys ignored the effects of structural relaxation, but subsequent developments of the theory, notably by Borie (1957, 1959), Cowley (1968), Borie & Sparks (1971) and Hayakawa & Cohen (1975), included the effects of structural relaxation and hence were also able to provide a description of these effects.

The purpose of this paper is twofold: firstly to report the experimental observation of another feature in diffraction patterns due to the effect of atomic size - namely the existence of a very characteristic and well defined absence of diffuse intensity along certain planes of reciprocal space - and secondly to provide an interpretation of this observation.

2. Example systems

Two recent examples of planar diffuse absences from our own work are shown in Figs. 1 and 2. Fig. 1 shows a grey-scale image of the reciprocal section $0{\cdot}4c^*$ of a cubic yttria stabilized zirconia ($Zr_{0.61}Y_{0.39}O_{1.805}$) measured using a single-crystal X-ray diffractometer system equipped with a position-sensitive detector (Osborn & Welberry, 1990). This pattern is obviously very complex with a whole variety of different and distinctive features. It is not our purpose in this paper to focus upon disorder in Y_2O_3-stabilized zirconia (this will be done elsewhere) but rather to concentrate upon the very distinctive ⟨110⟩ dark lines (*i.e.* lines where the diffuse intensity is absent), which can be shown, by comparison with other reciprocal sections, to result from the intersection of dark planes normal to ⟨110⟩. This is the direction that connects nearest-neighbour metal atoms in stabilized cubic zirconia.

0108-7673/92/050737-10$06.00

Similar features can be seen in Fig. 2, which displays an electron diffraction pattern taken approximately 7° from the [010] subcell zone axis of the incommensurately modulated Ta_2O_5.7%(WO_3) solid solution (Schmid, Withers & Thompson, 1992).

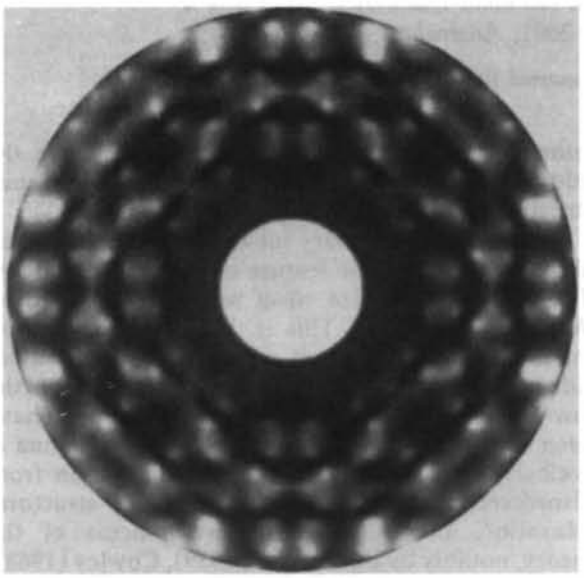

Fig. 1. The $0.4c^*$ diffuse-scattering section of a cubic stabilized zirconia ($Zr_{0.61}Y_{0.39}O_{1.81}$) measured using Cu $K\alpha$ X-radiation. $\mathbf{a}^*$ is horizontal and $\mathbf{b}^*$ is vertical. Note the dark lines running along ⟨110⟩ directions, which correspond to diffuse scattering absences on planes normal to ⟨110⟩.

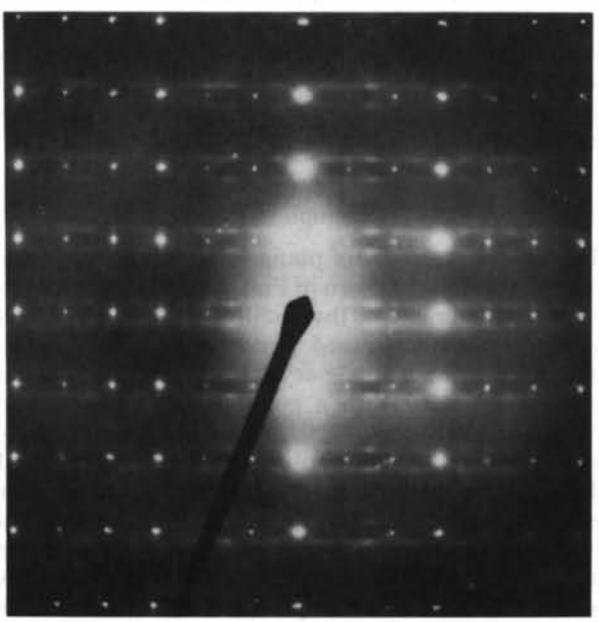

Fig. 2. An electron diffraction pattern taken approximately 7° off the [010] subcell zone axis of (Ta_2O_5).7%(WO_3). The $\mathbf{c}^*$ axis is vertical. Note the two diffuse sheets of intensity perpendicular to $\mathbf{c}^*$ surrounding a region where the diffuse intensity is absent.

Notice the characteristic diffuse intensity distribution consisting of two diffuse sheets of intensity perpendicular to [001] - a direction that connects nearest-neighbour metal atoms in this material - split on either side of the dark $\mathbf{G}\pm 0\mathbf{c}^*$ planes of reciprocal space.

A Monte Carlo simulation and optical-diffraction study by one of us (Welberry, 1986) on the atomic size effect in a hypothetical disordered two-dimensional binary alloy found an analogous effect - diffuse absences along lines in the diffraction pattern normal to the directions connecting nearest neighbours. These features were, however, only clearly visible in patterns where the scattering power of the two species were made identical. As an aid to the current investigation, this simulation was repeated but this time halted after fewer Monte Carlo steps, as this creates more pronounced diffuse absences.

Distortions were applied to the hypothetical alloy by assuming a preferred near-neighbour distance for *AA*-, *AB*- and *BB*-type pairs of the form

$$r_{AA} = a_0(1+\varepsilon_{AA}), \qquad r_{AB} = a_0(1+\varepsilon_{AB}), \qquad r_{BB} = a_0(1+\varepsilon_{BB}), \tag{1}$$

where a_0 is the lattice parameter and ε_{AA}, ε_{AB} and ε_{BB} were chosen to be +0.05, 0.0 and −0.05 respectively. The atom positions were allowed to relax off their ideal lattice sites using local energies derived from a Hooke's law force model that tends to restore atom pairs to these preferred distances. A two-dimensional square lattice of dimension 512×512 unit cells with concentration $c_A = 0.5$ was used. The *A* and *B* atoms were randomly placed on the lattice so as to avoid ordering effects in the diffraction pattern and 50 Monte Carlo steps at 'zero temperature' were performed. A Monte Carlo step is defined by each atom being visited in the simulation once on average. (For full details of the Monte Carlo simulation see Welberry, 1986.)

Fig. 3 shows a diffuse scattering pattern that was calculated by using a method that involves direct Fourier summation over all atoms in the simulation (Butler & Welberry, 1992). In the calculation, atom positions are accurate to 0.1% of the cell dimension and scattering factors of Zn and Cu were used respectively for the *A* and *B* atoms (a choice made simply because Cu and Zn, like Zr-Y and Ta-W, differ in scattering power by a single electron). This computed pattern is dominated by narrow dark lines running along rows of Bragg reflections, perpendicular to the directions connecting near neighbours and highlighted on either side by bands of enhanced diffuse intensity - much like the examples of Figs. 1 and 2 - indicating that the diffuse absences in all three patterns arise from similar processes.

The origin of this aspect of the atomic size effect can best be explained by concentrating on this two-

dimensional simulated alloy for which it is possible to isolate some of the contributions to the resultant diffraction pattern, for example, the purely displacive contribution, from those dependent on local ordering. Two distinct methods of description are employed here, a real-space (correlation) approach and a reciprocal-space (modulation-wave) approach.

3. Theoretical approaches

Two basic theoretical approaches are commonly used for describing disordered materials. The first is a real-space approach based upon a correlation or local-order description of disorder as commonly used, for example, in studies of alloys (Cenedese, Bley & Lefebvre, 1984; Matsubara & Cohen, 1985). The second is a reciprocal-space approach based upon the notion of compositional and displacive modulation waves (Krivoglaz, 1969; de Fontaine, 1972, 1973). Generally speaking, either approach should be capable of describing the same phenomena. In a specific case, however, there may well be arguments (such as the sharpness or otherwise of the diffuse features in reciprocal space) to suggest that one or other approach might be more appropriate or give more insight (Welberry & Withers, 1990).

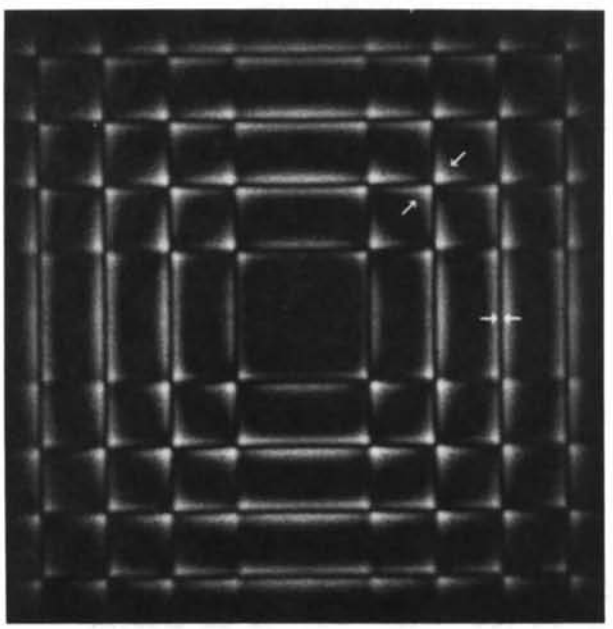

Fig. 3. Computed diffraction pattern (using direct Fourier summation techniques) of a two-dimensional square-lattice Monte Carlo simulation of size-effect distortions in a binary alloy. X-ray scattering factors of Cu and Zn were used for the two atom types. This figure demonstrates two diffuse features expected from alloys with size-effect distortions: diffuse absences on planes normal to the near-neighbour directions in the alloy (highlighted by the two horizontal arrows), and 'bow-tie'-like features most prominent along directions where $h_1 = h_2$ (highlighted by arrows at 45° to the horizontal).

The mathematical notation differs somewhat for the two approaches, following the conventions adopted in the current literature. The primary difference is in the labelling of the reciprocal coordinates, where continuous variables h_1, h_2 and h_3 are used in the correlation approach and the sum of a reciprocal-lattice vector, **G**, and a vector, **q**, inside the first Brillouin zone is used in the modulation-wave approach.

3.1. *A correlation approach*

A general description of diffuse scattering that allows for both short-range compositional order and local atomic distortions can be obtained (following Borie & Sparks, 1971) by expanding the exponential in the kinematic scattering equation to second moments in displacement:

$$I = \sum_{m=1}^{N}\sum_{n=1}^{N} f_m f_n \exp\left[i\mathbf{k}\cdot(\mathbf{R}_m+\mathbf{u}_m-\mathbf{R}_n-\mathbf{u}_n)\right]$$
$$\simeq \sum_{m=1}^{N}\sum_{n=1}^{N} f_m f_n \exp\left[i\mathbf{k}\cdot(\mathbf{R}_m-\mathbf{R}_n)\right]$$
$$\times\{1+i\mathbf{k}\cdot(\mathbf{u}_m-\mathbf{u}_n)-\tfrac{1}{2}[\mathbf{k}\cdot(\mathbf{u}_m-\mathbf{u}_n)]^2\}. \quad (2)$$

Here, I is the scattered intensity and f_m is the scattering factor of the atom (m) associated with a lattice site at the location $\mathbf{R}_m$ and which is displaced from its site by the small amount $\mathbf{u}_m$. For a binary alloy the diffuse scattered intensity, I_D, can be derived from (2) (Schwartz & Cohen, 1987). Following the notation of Georgopoulos & Cohen (1977) and restricting the form to two dimensions, we have

$$I_D(h_1,h_2) = c_A c_B (f_A-f_B)^2\{I_{\mathrm{SRO}} + h_1(\eta Q_x^{AA}+\zeta Q_x^{BB})$$
$$+ h_2(\eta Q_y^{AA}+\zeta Q_y^{BB})$$
$$+ h_1^2(\eta^2 R_x^{AA}+2\eta\zeta R_x^{AB}+\zeta^2 R_x^{BB})$$
$$+ h_2^2(\eta^2 R_y^{AA}+2\eta\zeta R_y^{AB}+\zeta^2 R_y^{BB})$$
$$+ h_1 h_2(\eta^2 S_{xy}^{AA}+2\eta\zeta S_{xy}^{AB}+\zeta^2 S_{xy}^{BB})\}, \quad (3)$$

where h_1 and h_2 are continuous reciprocal-space coordinates, c_A and c_B are the atomic concentrations of the A- and B-type atoms, η and ζ are scattering-factor ratios,

$$\eta = f_A/(f_A-f_B), \quad \zeta = f_B/(f_A-f_B), \quad (4)$$

and the component intensities are given by the sums

$$I_{\mathrm{SRO}} = \sum_l\sum_m \alpha_{lm}^{AB}\cos(2\pi h_1 l)\cos(2\pi h_2 m), \quad (5a)$$

$$Q_x^{AA} = -2\pi\sum_l\sum_m (c_A/c_B+\alpha_{lm}^{AB})\langle x_{lm}^{AA}\rangle$$
$$\times\sin(2\pi h_1 l)\cos(2\pi h_2 m), \quad (5b)$$

$$R_x^{AA} = 4\pi^2\sum_l\sum_m (c_A/c_B+\alpha_{lm}^{AB})\langle x_o^A x_{lm}^A\rangle$$
$$\times\cos(2\pi h_1 l)\cos(2\pi h_2 m), \quad (5c)$$

$$R_x^{AB} = 4\pi^2 \sum_l \sum_m (1-\alpha_{lm}^{AB})\langle x_o^A x_{lm}^B\rangle \times \cos(2\pi h_1 l)\cos(2\pi h_2 m), \quad (5d)$$

$$S_{xy}^{AA} = -8\pi^2 \sum_l \sum_m (c_A/c_B + \alpha_{lm}^{AB})\langle x_o^A y_{lm}^A\rangle \times \sin(2\pi h_1 l)\sin(2\pi h_2 m) \quad (5e)$$

etc. α_{lm}^{AB} are the Warren–Cowley short-range-order parameters, $\langle x_{lm}^{AA}\rangle$ is the average difference between displacements (along x) of an A-type atom at the end of a lattice vector (lm) and that of an A atom at its origin and $\langle x_o^A y_{lm}^A\rangle$ is the average value of the product of the displacement along x of an A atom at the origin of a lattice vector (lm) and the displacement along y of an A atom at the end of the vector. The intensity I_{SRO} thus describes the diffuse scattering associated with local chemical correlations, the intensity components involving Q terms describe scattering due to correlations between the average length of an interatomic vector and the occupation of the sites at the ends of the vector and those involving the R and S sums describe diffuse features associated with correlations in displacement of atom pairs separated by a lattice vector (lm). Inspection of (3) and (4) demonstrates that both the short-range-order diffuse scattering, I_{SRO}, and the Warren size-effect scattering, given by the Q intensity components, vanish with the scattering-factor difference $(f_A - f_B)$. For alloys in which the scattering is mainly associated with atoms that have similar atomic scattering factors, as is the case for the three examples given in this paper, the diffuse intensities associated with R and S terms will dominate the measured diffraction pattern.

To demonstrate the origins of the dark lines observed in the diffraction patterns of Figs. 1 and 2, we will concentrate on the simple two-dimensional structural simulation from which the diffraction pattern of Fig. 3 is derived and which shows clearly this same diffraction effect.

Equations (3) and (5) can be written for this case by setting the order parameters, α_{lm}^{AB}, to zero and neglecting those terms that depend on differences in the scattering factors,

$$I_D(h_1, h_2) = 4\pi^2 f^2 \{h_1^2 R_x' - 2h_1 h_2 S_{xy}' + h_2^2 R_y'\}, \quad (6)$$

where

$$R_x' = \sum_l \sum_m [c_A^2\langle x_o^A x_{lm}^A\rangle + 2c_A c_B\langle x_o^A x_{lm}^B\rangle + c_B^2\langle x_o^B x_{lm}^B\rangle] \times \cos(2\pi h_1 l)\cos(2\pi h_2 m), \quad (7a)$$

$$S_{xy}' = \sum_l \sum_m [c_A^2\langle x_o^A y_{lm}^A\rangle + 2c_A c_B\langle x_o^A y_{lm}^B\rangle + c_B^2\langle x_o^B y_{lm}^B\rangle] \times \sin(2\pi h_1 l)\sin(2\pi h_2 m), \quad (7b)$$

$$R_y' = \sum_l \sum_m [c_A^2\langle y_o^A y_{lm}^A\rangle + 2c_A c_B\langle y_o^A y_{lm}^B\rangle + c_B^2\langle y_o^B y_{lm}^B\rangle] \times \cos(2\pi h_1 l)\cos(2\pi h_2 m). \quad (7c)$$

It is possible to compute the diffraction pattern from the two-dimensional simulated alloy of Fig. 3 by simply substituting the values of all correlation parameters into (7), but this process would not help in understanding the origin of these observed diffraction effects. Instead, a more limited number of correlation parameters, whose values are indicative of general distortion effects, should be concentrated upon.

Consider the diffuse scattering along the reciprocal line $h_2 = 0$, which is a section normal to, and which passes through, some of the 'dark lines' in Fig. 3. For this section, (6) and (7) reduce to

$$I_D(h_1, 0) = 4\pi^2 f^2 h_1^2 \sum_l \sum_m [c_A^2\langle x_o^A x_{lm}^A\rangle + 2c_A c_B\langle x_o^A x_{lm}^B\rangle + c_B^2\langle x_o^B x_{lm}^B\rangle]\cos(2\pi h_1 l). \quad (8)$$

The origins of the dark lines in Fig. 3 and thus the dark planes of the stabilized zirconia and tantalum tungstate diffraction patterns must lie in the behaviour of the correlation parameters $\langle x_o^A x_{lm}^A\rangle$, $\langle x_o^A x_{lm}^B\rangle$, $\langle x_o^B x_{lm}^B\rangle$ since these features pass through the reciprocal section described by (8). Although this equation implies summation over all possible interatomic vectors (lm), the contribution from large vectors will tend toward zero (since correlations responsible for diffuse intensities are by definition local). Of the shorter vectors remaining it might be expected that only a few will be responsible for the observed diffraction effects. The diffuse intensity, composed of only a small number of such correlations, could be easily described using this approach.

From the Monte Carlo simulated structure it is possible to compute the displacement correlations contributing to the intensity and so determine directly which ones are large and thus responsible for the dark lines. In Table 1(*a*) a listing of the three correlation coefficients contained in (8) (normalized such that the self correlation is unity) as a function of the interatomic vector is presented. Correlations for all lattice vectors out to $(l, m) = (10, 10)$ were computed but only those that are greater than 1% are presented. Essentially, the only nonzero strain correlations are those with interatomic vectors along the direction that the Hooke's law force acts. Only two vectors not along the direction $m = 0$ have values greater than 1% [the (0, 1) and (1, 1) vectors] but these are quite small. Correlations along the $m = 0$ direction are large for nearest $(l, 0)$ vectors and fall off gradually until vanishing around $(l, m) = (10, 0)$. In the last column of Table 1(*a*) the term in square brackets in (8) - the coefficient of the cosine function - has been computed.

We see that the first and second cosine coefficients are relatively large and positive and the rest are negative and decay in magnitude until disappearing at about $(l, m) = (10, 0)$. The first two positive coefficients will contribute broad diffuse peaks of

intensity centred about integer values of h_1 and the string of negative coefficients will subtract intensity from the centre of these diffuse peaks. We are thus left with diffuse bands around integer h_1 positions and dark lines that run down the middle of these bands. This fact is demonstrated in Fig. 4, where the cosine summation of (8) has been computed using only the 12 coefficients presented in the last column of Table 1(*a*). This can be compared with the diffuse intensity computed exactly by direct Fourier summation over the entire simulated crystal using the method of Butler & Welberry (1992), which does not suffer from any of the approximations made in deriving (3). (In both of these computations, f_A and f_B were taken to be that of Cu to avoid any influence from the Laue monotonic and Warren size-effect intensities.) The broad diffuse maxima with sharp reduction in intensity at integer reciprocal positions can be clearly seen. Qualitatively, this correlation approach describes very well the dark lines in this diffraction pattern and, except for the height of the diffuse bands on either side of the dark line, the quantitative agreement is good as well. The approximation made in truncating the exponential at second moments in displacement is responsible for any differences,* so if atomic distortions smaller than the 3.5% (root-mean-square) average of this particular simulation were used, the quantitative differences would be less pronounced.

We now demonstrate why this simple force model produces displacement correlations with the observed behaviour. A negative value of the displacement correlation $\langle x_o^A x_{l0}^B \rangle$ implies that, on average, atoms A and B separated by the lattice vector $(l, 0)$ tend to move either away (as shown in Fig. 5*a*) or toward each other along the x direction, while a positive correlation means that, on average, the atoms tend to move together in either the $+x$ or $-x$ direction (Fig. 5*b*). In the simulated distorted crystal we see from Table 1(*a*) that near-neighbour pairs tend to move together, while the more distant pairs, along the direction of the Hooke's law force, tend to move in opposite directions regardless of the identity of the atoms that form the pair. This peculiar behaviour can be explained by considering the local environment of the atoms forming a pair.

On either side of a pair of atoms that are near neighbours there will, on average, be a statistical local excess of 'larger' A atoms or 'smaller' B atoms which will tend, respectively, to push the atom pair away from or pull the atom pair toward the region that contains the excess. In either case, the result is a positive displacement correlation as can be seen from

* Including the rest of the small correlation parameters will change the computed pattern only slightly.

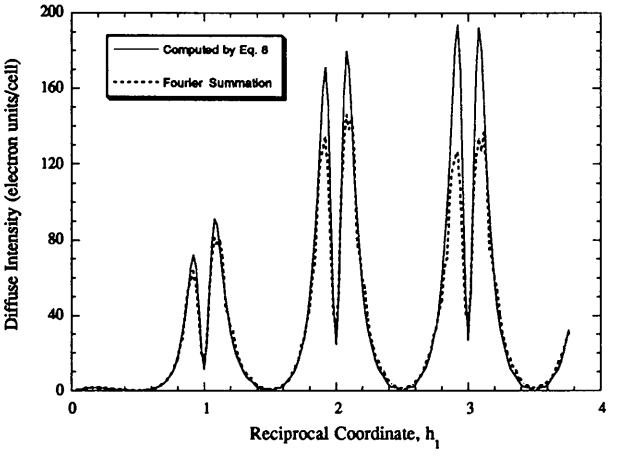

Fig. 4. The diffuse intensity associated with the Monte Carlo simulated alloy computed using the correlation parameters of Table 1(*a*) and (8) (based on an expansion of the kinematic scattering equation to second order in displacement). The dashed line represents an exact calculation of the diffuse intensity using a direct Fourier summation technique.

Table 1. *Correlation parameters from the simulated binary alloy that apply to (a) R_x and (b) S_{xy} diffuse intensity components*

The last column shows the computed value of the term in square brackets in equation (8). Note that

$$\overline{\langle x_o^A y_{lm}^B \rangle} = \langle x_o^B y_{lm}^B \rangle / [\langle (x^A)^2 \rangle \langle (y^B)^2 \rangle]^{1/2}$$

etc. and

$$[\,] = [c_A^2 \langle x_o^A y_{lm}^A \rangle + 2 c_A c_B \langle x_o^A y_{lm}^B \rangle + c_B^2 \langle x_o^B y_{lm}^B \rangle].$$

The values of $\langle (x^A)^2 \rangle$ and $\langle (x^B)^2 \rangle$ for this simulated crystal are 12.0 and $11.5 \times 10^{-4} a_0^2$ respectively.

(*a*) R_x

l, m	$\overline{\langle x_o^A x_{lm}^B \rangle}$	$\overline{\langle x_o^A x_{lm}^A \rangle}$	$\overline{\langle x_o^B x_{lm}^B \rangle}$	$[\,]$ $(\times 10^4 a_0^2)$
1, 0	+0.92	+0.38	+0.35	+7.60
2, 0	+0.23	−0.01	−0.02	+1.28
3, 0	−0.11	−0.20	−0.20	−1.80
4, 0	−0.21	−0.25	−0.25	−2.73
5, 0	−0.21	−0.22	−0.22	−2.55
6, 0	−0.17	−0.17	−0.16	−1.96
7, 0	−0.12	−0.12	−0.11	−1.36
8, 0	−0.07	−0.08	−0.07	−0.85
9, 0	−0.04	−0.04	−0.03	−0.48
10, 0	−0.02	−0.02	−0.02	−0.23
0, 1	+0.00	−0.03	+0.03	+0.00
1, 1	−0.00	−0.01	+0.02	+0.02

(*b*) S_{xy}

l, m	$\overline{\langle x_o^A y_{lm}^B \rangle}$	$\overline{\langle x_o^A y_{lm}^A \rangle}$	$\overline{\langle x_o^B y_{lm}^B \rangle}$	$[\,]$ $(\times 10^4 a_0^2)$
1, 1	−0.28	−0.28	−0.27	−3.29
2, 1	−0.18	−0.19	−0.19	−2.17
3, 1	−0.11	−0.10	−0.12	−1.31
4, 1	−0.06	−0.06	−0.07	−0.74
5, 1	−0.04	−0.02	−0.04	−0.41
6, 1	−0.02	−0.01	−0.02	−0.23
2, 2	−0.12	−0.13	−0.13	−1.48
3, 2	−0.08	−0.07	−0.08	−0.91
4, 2	−0.04	−0.04	−0.04	−0.50
5, 2	−0.02	−0.02	−0.02	−0.26
3, 3	−0.05	−0.05	−0.05	−0.57
4, 3	−0.02	−0.03	−0.03	−0.31
4, 4	−0.02	−0.01	−0.02	−0.17

the values in the first row of Table 1(*a*). Likewise, a negative displacement correlation will exist for pairs separated by longer distances since an excess of *A* atoms or *B* atoms in the intervening region will cause the pair to move away from or toward each other.

In the simulation presented here, the crossover between positive and negative displacement correlations occurs at $(l, m) = (2, 0)$ and negative correlations persist out to approximately $(l, m) = (10, 0)$. Since (8) involves a summation of cosine terms with arguments proportional to the interatomic vector length, the sharpness of the dark line is determined by the extent of negative correlation and the breadth of the diffuse bands on either side depends on the number of nearest-neighbour correlations that are positive. For example, an alloy in which positive displacive correlations persist for many neighbours, with few negative correlations, will show a relatively broad dark line and sharp diffuse bands on either side, whereas an alloy with few positive correlations and many negative correlations (like the Monte Carlo simulation) will display sharp dark lines and broad diffuse bands. The relative widths of the diffuse bands and dark lines will thus depend on the detailed atomic interactions in the alloy considered, but the existence of a dark line with diffuse bands on either side should be a *characteristic feature* of all alloys with 'size-effect'-like distortions. In systems where neighbouring atoms are connected by lattice vectors not along the cell axes, the *R* and *S* sums will mix to produce diffuse absences along the direction connecting neighbours in the lattice. In such cases, (8) can still be used to demonstrate directly the diffuse absences by simply reindexing the pattern so that the crystallographic axes coincide with near-neighbour directions.

If the displacive correlations, $\langle x_o x_{lm}\rangle$, where $m = 0$ (and by symmetry the correlations, $\langle y_o y_{lm}\rangle$, with $l = 0$) are the only nonzero correlations in the simulated crystal then the diffraction pattern displays only dark lines perpendicular to the near-neighbour directions thus forming dark 'squares'. There is, however, another feature in the computed pattern of Fig. 3 - 'bow tie'-like figures running along the $\langle 11\rangle$ directions and lying near the intersection of the dark lines. This must result from the set of correlations associated with the S_{xy} intensity component of (6) since all the $\langle x_o x_{lm}\rangle$ correlations have been accounted for. The displacive correlations, $\langle x_o y_{lm}\rangle$, were computed directly from the simulated crystal and are presented in Table 1(*b*). These were computed for interatomic vectors out to $(l, m) = (10, 10)$ but only those greater than 2% are listed. All of the large $\langle x_o y_{lm}\rangle$ correlations are found to be negative and, of these, the largest are for atom pairs separated by the vector $(l, m) = (1, 1)$.

A negative $\langle x_o y_{lm}\rangle$ correlation means that the x displacement of an atom at the origin of a lattice vector (l, m) moves with opposite sign to the y displacement of the atom at the end of the vector. This is demonstrated in Fig. 5(*c*) for an *AB* pair separated by $(l, m) = (1, 1)$. In this case, the negative correlation is shown to result from both the *A* and *B* atoms moving away from the mutually shared near-neighbour site. Motions of the *A* and *B* atoms toward this site would also result in a negative value of $\langle x_o y_{lm}\rangle$. Such correlations *are* expected from an alloy with size-effect-like distortions regardless of the type of atoms at the ends of the vector (1, 1) as a 'large' *A* atom at the shared near-neighbour site would tend to move both atoms outward and a 'small' *B* atom would tend to draw the atoms inward. Both cases correspond to negative $\langle x_0 y_{lm}\rangle$ correlation. A similar argument holds for the other pairs in Table 1(*b*).

The intensity component, S_{xy}, involves a sum of sine functions so its effect is to transfer diffuse intensity from one side of the lines l = integer or m = integer to the other with maximum effect near $h_1 = h_2$. Negative coefficients to these sine functions will produce 'bow tie' figures along the direction $\langle 11\rangle$ near the intersections of 'dark lines' (as we find in Fig. 3) because intensity from the diffuse bands will be transferred from the high-angle to the low-angle sides of the dark lines enhancing the observed intensity along the $h_1 = h_2$ direction. This mechanism is also expected to operate characteristically in other alloys that relax through size-effect-like distortions. Indeed, in the stabilized zirconia example of Fig. 1 we do observe 'bow-tie'-like figures at the intersection of the dark lines, however, these are oriented at right angles to the ones in the simulation of the size effect. Bow-tie figures in this orientation will result from positive $\langle x_o y_{lm}\rangle$ correlations, like that demonstrated in Fig. 5(*d*). For a discussion of why these correlations are positive in the stabilized zirconia see Welberry, Withers, Thomson & Butler (1992).

3.2. *A modulation-wave approach*

An equally general description of diffuse scattering can be obtained *via* a modulation-wave or reciprocal-space approach. Let μ label the independent sites per average structure primitive unit cell, $\mathbf{T}$ the position of the particular primitive unit cell, $\bar{f}_\mu$ the atomic scattering factor of the μth site in the average structure and $\mathbf{T}+\mathbf{r}_\mu$ the position of the μth site in the average structure. Any arbitrary ordering scheme and associated structural relaxation can be described in terms of such an average structure plus compositional and displacive modulations of the form

$$\begin{aligned}\delta f_\mu(\mathbf{T}) &= \bar{f}_\mu \sum_{q_c} a_\mu(\boldsymbol{q}_c) \exp\{2\pi i \mathbf{q}_c \cdot \mathbf{T}\} \\ \mathbf{u}_\mu(\mathbf{T}) &= \sum_{q_d} e_\mu(\mathbf{q}_d) \exp\{2\pi i \mathbf{q}_d \cdot \mathbf{T}\},\end{aligned} \tag{9}$$

where $a_\mu(-\mathbf{q}_c) = a_\mu(\mathbf{q}_c)^*$, $\mathbf{e}_\mu(-\mathbf{q}_d) = \mathbf{e}_\mu(\mathbf{q}_d)^*$ and where the summations over $\mathbf{q}_c$ and $\mathbf{q}_d$ (c for compositional modulation and d for displacive modulation)

are understood to range over the whole of the first Brillouin zone. The structure-factor amplitude, $F(\mathbf{k})$, is thus given by

$$F(\mathbf{k}) = \sum_{\mu}\sum_{\mathbf{T}} [\bar{f}_\mu + \delta f_\mu(\mathbf{T})] \times \exp\{-2\pi i\mathbf{k}\cdot[\mathbf{T}+\mathbf{r}_\mu+u_\mu(\mathbf{T})]\}. \quad (10)$$

Using the Jacobi–Auger generating relation plus other standard mathematical procedures (see, for example, Perez-Mato, Madariaga & Tello, 1986) and expanding to second order in modulation-wave amplitudes [the modulation-wave analogue of the second-moment expansion of (2)], one can break down the diffracted intensity $I(\mathbf{k})$ into four parts:

$$\begin{aligned}
I_1(\mathbf{G}) &= N^2 \sum_{\mu}\sum_{\mu'} f_\mu f_{\mu'} \exp\{-2\pi i\mathbf{G}\cdot(\mathbf{r}_\mu-\mathbf{r}_{\mu'})\} \\
&\quad\times\Big[1-\tfrac{1}{4}\sum_{q}\{|2\pi\mathbf{G}\cdot\mathbf{e}_\mu(\mathbf{q})|^2 \\
&\quad+|2\pi\mathbf{G}\cdot\mathbf{e}_{\mu'}(\mathbf{q})|^2\}\Big] \\
I_2(\mathbf{G}+\mathbf{q}) &= N^2 \sum_{\mu}\sum_{\mu'} \bar{f}_\mu \bar{f}^*_{\mu'} \\
&\quad\times\exp\{-2\pi i(\mathbf{G}+\mathbf{q})\cdot(\mathbf{r}_\mu-\mathbf{r}_{\mu'})\} \\
&\quad\times a_\mu(\mathbf{q}) a_{\mu'}(\mathbf{q})^* \\
I_3(\mathbf{G}+\mathbf{q}) &= \tfrac{1}{2}N^2 \sum_{\mu}\sum_{\mu'} \bar{f}_\mu \bar{f}^*_{\mu'} \\
&\quad\times\exp\{-2\pi i(\mathbf{G}+\mathbf{q})\cdot(\mathbf{r}_\mu-\mathbf{r}_{\mu'})\} \\
&\quad\times[2\pi(\mathbf{G}+\mathbf{q})\cdot\mathbf{e}_\mu(\mathbf{q})] \\
&\quad\times[2\pi(\mathbf{G}+\mathbf{q})\cdot\mathbf{e}_{\mu'}(\mathbf{q})^*] \\
I_4(\mathbf{G}+\mathbf{q}) &= N^2 \sum_{\mu}\sum_{\mu'} \bar{f}_\mu \bar{f}^*_{\mu'} \\
&\quad\times\exp\{-2\pi i\,(\mathbf{G}+\mathbf{q})\cdot(\mathbf{r}_\mu-\mathbf{r}_{\mu'})\} \\
&\quad\times[2\pi\, a_\mu(\mathbf{q})(\mathbf{G}+\mathbf{q})\cdot\mathbf{e}_\mu(\mathbf{q})^*\exp\{i\pi/2\} \\
&\quad+2\pi a_{\mu'}(\mathbf{q})^*\,(\mathbf{G}+\mathbf{q})\cdot\mathbf{e}_{\mu'}(\mathbf{q})\exp\{-i\pi/2\}].
\end{aligned} \quad (11)$$

The intensity I_1 is independent of the atomic ordering although not of the associated structural relaxation and gives rise to the sharp Bragg reflections of the average structure. The three further contributions I_2, I_3 and I_4 give rise to the diffuse features of reciprocal space. The short-range-order term I_2 depends solely upon the extent of compositional ordering while the displacive term I_3 depends solely upon the extent of displacive modulation or structural relaxation. The final part, the 'size-effect' term I_4, arises from the correlation or coupling between the compositional and displacive modulations and gives rise to the well known and characteristic effect of transferring intensity from regions on one side of Bragg reflections to regions on the other.

If there is only one atom per primitive unit cell, as in binary substitutional alloys, these equations can be further reduced to give

$$\begin{aligned}
I_1(\mathbf{G}) &= N^2|\bar{f}^2|\Big[1-\tfrac{1}{2}\sum_{q}|2\pi\mathbf{G}\cdot\mathbf{e}(\mathbf{q})|^2\Big] \\
I_2(\mathbf{G}+\mathbf{q}) &= N^2|\bar{f}^2||a(\mathbf{q})|^2 \\
I_3(\mathbf{G}+\mathbf{q}) &= \tfrac{1}{2}N^2|\bar{f}^2||2\pi(\mathbf{G}+\mathbf{q})\cdot\mathbf{e}(\mathbf{q})|^2 \\
I_4(\mathbf{G}+\mathbf{Q}) &= 2N^2|\bar{f}^2|\Re\mathrm{e}\{2\pi\, a(\mathbf{q})(\mathbf{G}+\mathbf{q})\cdot\mathbf{e}(\mathbf{q})^* \\
&\quad\times\exp[i\pi/2]\}.
\end{aligned} \quad (12)$$

The latter three terms are the modulation-wave analogue of (3)–(5) above. $I_2(\mathbf{G}+\mathbf{q})$ corresponds to the I_{SRO} term given in (5a), $I_3(\mathbf{G}+\mathbf{q})$ to those intensity components involving R and S terms and $I_4(\mathbf{G}+\mathbf{q})$ to those intensity components involving Q terms.

From a modulation-wave point of view, further progress requires the correlation of the displacive modulation-wave amplitudes [the $\mathbf{e}(\mathbf{q})$'s] with the corresponding compositional modulation-wave amplitudes [the $a(\mathbf{q})$'s]. How this should be done is suggested by the Monte Carlo simulation described in the previous section. In the 'first-order size effect' described by Welberry (1986), each atom is allowed to shift from its mean lattice-site position to alleviate the size-effect strain with its nearest neighbours only. In modulated-structure language this is equivalent to the statement that

$$\mathbf{u}(\mathbf{T}) \propto \mathbf{a}\{\delta f(\mathbf{T}-\mathbf{a})-\delta f(\mathbf{T}+\mathbf{a})\} + \mathbf{b}\{\delta f(\mathbf{T}-\mathbf{b})-\delta f(\mathbf{T}+\mathbf{b})\}, \quad (13)$$

which, in turn, implies that

$$\mathbf{e}(\mathbf{q}) \propto a(\mathbf{q})\exp\{-i\pi/2\}\{\mathbf{a}\sin(2\pi\mathbf{q}\cdot\mathbf{a}) + \mathbf{b}\sin(2\pi\mathbf{q}\cdot\mathbf{b})\}, \quad (14)$$

where $\mathbf{a}$ and $\mathbf{b}$ are the unit-cell axes. Within the limits of validity of this first-order approximation to the correct relationship between $\mathbf{e}(\mathbf{q})$ and $a(\mathbf{q})$, it holds that

$$I_4(\mathbf{G}+\mathbf{q}) \propto -|a(\mathbf{q})|^2(\mathbf{G}+\mathbf{q})\cdot\{\mathbf{a}\sin(2\pi\mathbf{q}\cdot\mathbf{a}) + \mathbf{b}\sin(2\pi\mathbf{q}\cdot\mathbf{b})\}, \quad (15a)$$

while

$$I_4(\mathbf{G}-\mathbf{q}) \propto +|a(\mathbf{q})|^2(\mathbf{G}-\mathbf{q})\cdot\{\mathbf{a}\sin(2\pi\mathbf{q}\cdot\mathbf{a}) + \mathbf{b}\sin(2\pi\mathbf{q}\cdot\mathbf{b})\}. \quad (15b)$$

This is the modulation-wave approach analogue of the Q_x terms of the real-space approach of the previous section and is the mathematical equivalent of Fig. 1(e) of Welberry (1986), *i.e.* intensity is transferred from the high-angle side of the Bragg reflections to the low-angle side as required.

Note, furthermore, that

$$e_x(\mathbf{q}) \propto a(\mathbf{q})\exp\{-i(\pi/2)\}\sin(2\pi\mathbf{q}\cdot\mathbf{a}) = 0$$

for $\mathbf{q}$ parallel to $\mathbf{b}^*$ and that $e_y(\mathbf{q})=0$ for $\mathbf{q}$ parallel to $\mathbf{a}^*$. Thus, a compositional modulation with modulation wave vector $\mathbf{q}$ exactly parallel to $\mathbf{b}^*$ can only induce a corresponding displacive modulation polarized along $\mathbf{b}$, *i.e.* no corresponding structural relaxation along $\mathbf{a}$ is allowed. This can be qualitatively rationalized as follows. A compositional modulation with modulation wave vector $\mathbf{q}$ exactly parallel to $\mathbf{b}^*$ must, of necessity, create rows of atom sites along $\mathbf{a}$ that contain more of either the large or small atoms. A corresponding structural relaxation along $\mathbf{a}$, therefore, would necessarily imply macroscopic strain and hence does not occur (*i.e.* has zero amplitude). Since $I_3(\mathbf{G}+\mathbf{q}) \propto |(\mathbf{G}+\mathbf{q})\cdot\mathbf{e}(\mathbf{q})|^2$, (14) also provides the basis for understanding the presence of the dark line in Fig. 3. Thus, within the limits of the above first-order approximation, the purely displacive contribution to the simulated diffraction pattern takes the form

$$\begin{aligned} I_3(h+q_x, k+q_y) \propto & -|a(q_x, q_y)|^2[(h+q_x)\sin(2\pi q_x) \\ & +(k+q_y)\sin(2\pi q_y)]^2 \\ = & -|a(q_x, q_y)|^2 \\ & \times\{[(h+q_x)\sin(2\pi q_x)]^2 \\ & +[(k+q_y)\sin(2\pi q_y)]^2 \\ & +(h+q_x)(k+q_y) \\ & \times[\cos 2\pi(q_x-q_y) \\ & -\cos 2\pi(q_x+q_y)]\}. \end{aligned} \tag{16}$$

The first two terms in the above expression are the modulation-wave analogue of the R_x term of the real-space approach while the latter term corresponds to the S_{xy} term. Note that this latter term, for $h=k$, is maximized for $q_x=q_y$ while, for $k=-h$, it is maximized for $q_x=-q_y$. This provides the basis for understanding the origin and relative orientation of the 'bow ties' observed in the simulated diffuse distribution along the $h=k$ and $h=-k$ directions of reciprocal space. The simulated diffuse distribution, shown in Fig. 3, corresponds to the term I_3.

Further iteration, or relaxation, beyond the above first-order relaxation means that the displacement of any individual atom will become subject to influences extending beyond nearest neighbours. The most general extension of the above 'first-order' relationship between $\mathbf{u}(\mathbf{T})$ and $\delta f(\mathbf{T})$ is

$$\mathbf{u}(\mathbf{T}) = \sum_{\Delta T} \boldsymbol{\varepsilon}(\Delta\mathbf{T})\{\delta f(\mathbf{T}-\Delta\mathbf{T}) - \delta f(\mathbf{T}+\Delta\mathbf{T})\}, \tag{17}$$

where no assumption is made as to the magnitude or direction of the influence upon a particular atom at $\mathbf{T}$ due to neighbouring atoms at $\mathbf{T}+\Delta\mathbf{T}$ and $\mathbf{T}-\Delta\mathbf{T}$. Then

$$\mathbf{e}(\mathbf{q}) = a(\mathbf{q})\exp\{-i(\pi/2)\}\sum_{\Delta T}\boldsymbol{\varepsilon}(\Delta\mathbf{T})\sin(2\pi\mathbf{q}\cdot\Delta\mathbf{T}). \tag{18}$$

In this general case, the 'size effect' term $I_4(\mathbf{G}+\mathbf{q})$ can be written in the form

$$I_4(\mathbf{G}+\mathbf{q}) = -2N^2\bar{f}^2 2\pi|a(\mathbf{q})|^2\sum_{\Delta T}(\mathbf{G}+\mathbf{q})\cdot\boldsymbol{\varepsilon}(\Delta\mathbf{T}) \times\sin(2\pi\mathbf{q}\cdot\Delta\mathbf{T}), \tag{19}$$

while the purely displacive term $I_3(\mathbf{G}+\mathbf{q})$ can be written as

$$\begin{aligned} I_3(\mathbf{G}+\mathbf{q}) = & \tfrac{1}{2}N^2\bar{f}^2 4\pi^2|a(\mathbf{q})|^2\sum_{\Delta T}(\mathbf{G}+\mathbf{q})\cdot\boldsymbol{\varepsilon}(\Delta\mathbf{T}) \\ & \times\sin(2\pi\mathbf{q}\cdot\mathbf{T}) \\ & \times\sum_{\Delta T'}(\mathbf{G}+\mathbf{q})\cdot\boldsymbol{\varepsilon}(\Delta\mathbf{T}')\sin(2\pi\mathbf{q}\cdot\Delta\mathbf{T}') \end{aligned} \tag{20}$$

or, after appropriate manipulation, in a form identical to that given in (6) above,

$$\begin{aligned} I_3(h_1, h_2) \propto & 4\pi^2\bar{f}^2\Big\{h_1^2\sum_l\sum_m\Big[\sum_{l'}\sum_{m'}\varepsilon_x(l', m') \\ & \times\varepsilon_x(l'-l, m'-m)\Big] \\ & \times\cos(2\pi h_1 l)\cos(2\pi h_2 m) \\ & +h_2^2\sum_l\sum_m\Big[\sum_{l'}\sum_{m'}\varepsilon_y(l', m') \\ & \times\varepsilon_y(l'-l, m'-m)\Big] \\ & \times\cos(2\pi h_1 l)\cos(2\pi h_2 m) \\ & +2h_1h_2\sum_l\sum_m\Big[\sum_{l'}\sum_{m'}\varepsilon_x(l', m') \\ & \times\varepsilon_y(l'-l, m'-m)\Big] \\ & \times\sin(2\pi h_1 l)\sin(2\pi h_2 m)\Big\}. \end{aligned} \tag{21}$$

Now, however, the terms R'_x, S'_{xy} and R'_y of §3.1 above (and tabulated in Tables 1 and 2) are functions of $\boldsymbol{\varepsilon}(\Delta\mathbf{T}=l\mathbf{a}+m\mathbf{b})$.

In reciprocal-space language, the observation of the dark line requires that the relationship between $\mathbf{u}(\mathbf{T})$ and $\delta f(\mathbf{T})$ takes the very specific form

$$\begin{aligned} \mathbf{u}(\mathbf{T}) = & \sum_m \mathbf{a}\varepsilon(m, 0)\{\delta f(\mathbf{T}-m\mathbf{a}) - \delta f(\mathbf{T}+m\mathbf{a})\} \\ & +\sum_n \mathbf{b}\varepsilon(0, n)\{\delta f(\mathbf{T}-n\mathbf{b}) - \delta f(\mathbf{T}+n\mathbf{b})\}, \end{aligned} \tag{22}$$

so that

$$\begin{aligned} \mathbf{e}(\mathbf{q}) = & a(\mathbf{q})\exp\{-i(\pi/2)\}[\mathbf{a}\{\varepsilon_x(1, 0)\sin(2\pi\mathbf{q}\cdot\mathbf{a}) \\ & +\varepsilon_x(2, 0)\sin(2\pi\mathbf{q}\cdot 2\mathbf{a})+\cdots\} \\ & +\mathbf{b}\{\varepsilon_y(0, 1)\sin(2\pi\mathbf{q}\cdot\mathbf{b}) \\ & +\varepsilon_y(0, 2)\sin(2\pi\mathbf{q}\cdot 2\mathbf{b})+\cdots\}]. \end{aligned} \tag{23}$$

Such an extension of the first-order relaxation maintains the property that $\varepsilon_x(\mathbf{q})=0$ for $\mathbf{q}$ parallel to $\mathbf{b}^*$ and that $\varepsilon_y(\mathbf{q})=0$ for $\mathbf{q}$ parallel to $\mathbf{a}^*$ and hence maintains the basis for understanding the presence of the dark line. It also provides a qualitative description of how the simulated diffuse distribution comes to be localized close to the $\mathbf{G}\pm q_x\mathbf{a}^*$ or $\mathbf{G}\pm q_y\mathbf{b}^*$ lines of reciprocal space, *i.e.* of why the observed diffuse intensity occurs where it does. That the $\varepsilon(\Delta\mathbf{T})$'s are nonzero only along the **a** and **b** directions in this simulated two-dimensional alloy appears to result from the simulated forces on the atoms acting purely along the lines of their centres as discussed above.

4. Discussion

In the previous sections we described, using both correlation-space and modulation-wave approaches, what aspects of the two-dimensional simulated alloy are responsible for the absence of diffuse intensity along particular lines in the diffraction pattern of Fig. 3. The basic mechanism responsible for these diffuse features is that atomic displacements act principally along the directions that connect nearest-neighbour sites and (in real-space language) are correlated positively for nearest-neighbour atom pairs and negatively for more distant pairs regardless of the types of atoms that form the pair. Although using Hooke's law forces that tend to restore atom pairs to preferred separation distances is an oversimplification for most materials, the basic forces at play in real systems should produce, qualitatively, the same kind of lattice relaxations. This should be the case in metallic alloys where nearest-neighbour interactions dominate the atomic displacements but also in more complicated systems, such as the two oxide examples of this paper, where more complicated atomic interactions act in concert to produce similar effects. These diffraction effects should, therefore, be characteristic of all systems in which such distortions act.

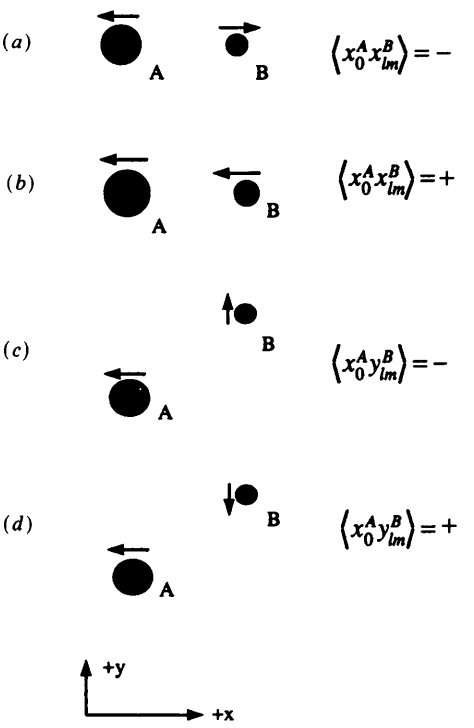

Fig. 5. One of the two possible pair distortions that result in (*a*) a negative $\langle x_o^A x_{lm}^B\rangle$ correlation, (*b*) a positive $\langle x_o^A x_{lm}^B\rangle$ correlation, (*c*) a negative $\langle x_o^A y_{lm}^B\rangle$ correlation and (*d*) a positive $\langle x_o^A y_{lm}^B\rangle$ correlation. Reversing the sign of both displacements in each of the four cases has no effect on the sign of the correlation parameters.

Why then have diffuse absences of this kind, which are natural manifestations of these distortions, not been reported previously? The answer lies with the fact that, historically, efforts have been concentrated on the determination of local chemical order in diffraction studies of disordered systems. In such studies the use of atomic species with large scattering-factor differences predominates as this greatly enhances the diffuse intensity due to short-range order. The normal Warren size-effect scattering (Warren, Averbach & Roberts, 1951), represented by the intensities associated with the Q sums of the correlation approach or the intensity component I_4 of the modulation-wave approach, depends on scattering-factor differences and so will also be large and thus hide the weaker scattering effects described here. Additionally, this size-effect scattering acts to transfer intensity from one side of the planes $h=$ integer to the other and so the diffuse band on one side of the dark line will be weakened at the expense of the band on the other, further obscuring the dark line. Indeed, if the scattering factors used in the computation of Fig. 3 were substantially different, the dark lines would not be visible at all, as demonstrated by Welberry (1986).

Furthermore, size-effect distortions tend to be small in alloys composed of neighbouring elements in the Periodic Table so in X-ray and electron diffraction studies of these alloys the diffuse absences might be difficult to observe. (Using neutron diffraction, however, it is possible to find atomic species with similar scattering length and dissimilar size). In the oxide examples of Figs. 1 and 2 it is likely that these effects result not from the actual difference in 'sizes' (which are small) but because the two metal atoms tend to coordinate with oxygen in different ways creating, effectively, large size differences. Examples of planar diffuse absences are, therefore, likely to be shown by other oxide materials.

The diffuse scattering image of Fig. 3 was computed on a Fujitsu VP-2200 supercomputer using a grant from the Australian National University Supercomputer Facility.

References

BORIE, B. (1957). *Acta Cryst.* **10**, 89-96.
BORIE, B. (1959). *Acta Cryst.* **12**, 280-282.
BORIE, B. & SPARKS, C. J. (1971). *Acta Cryst.* A**27**, 198-201.
BUTLER, B. D. & WELBERRY, T. R. (1992). *J. Appl. Cryst.* **25**, 391-399.
CENEDESE, P., BLEY, F. & LEFEBVRE, S. (1984). *Acta Cryst.* A**40**, 228-240.
COWLEY, J. M. (1968). *Acta Cryst.* A**24**, 557-563.
FONTAINE, D. DE (1972). *J. Phys. Chem. Solids*, **33**, 297-310.
FONTAINE, D. DE (1973). *J. Phys. Chem. Solids*, **34**, 1285-1304.
GEORGOPOULOS, P. & COHEN, J. B. (1977). *J. Phys. (Paris) Colloq.* 7, **38**, 191-196.
HAYAKAWA, M. & COHEN, J. B. (1975). *Acta Cryst.* A**31**, 635-645.
KHANNA, R. & WELBERRY, T. R. (1990). *Acta Cryst.* A**46**, 970-974.
KRIVOGLAZ, M. A. (1969). *Theory of X-ray and Thermal Neutron Scattering by Real Crystals.* New York: Plenum Press.
MATSUBARA, E. & COHEN, J. B. (1985). *Acta Metall.* **33**, 1945-1955.
OSBORN, J. C. & WELBERRY, T. R. (1990). *J. Appl. Cryst.* **23**, 476-484.
PEREZ-MATO, J. M., MADARIAGA, G. & TELLO, M. J. (1986). *J. Phys. C*, **19**, 2613-2622.
SCHMID, S., WITHERS, R. L. & THOMPSON, J. G. (1992). *J. Solid State Chem.* In the press.
SCHWARTZ, L. H. & COHEN, J. B. (1987). *Diffraction from Materials.* Berlin: Springer-Verlag.
WARREN, B. E., AVERBACH, B. L. & ROBERTS, B. W. (1951). *J. Appl. Phys.* **22**, 1493-1496.
WELBERRY, T. R. (1986). *J. Appl. Cryst.* **19**, 382-389.
WELBERRY, T. R. & WITHERS, R. L. (1990). *J. Appl. Cryst.* **23**, 303-314.
WELBERRY, T. R., WITHERS, R. L. & OSBORN, J. C. (1990). *Acta Cryst.* B**46**, 267-275.
WELBERRY, T. R., WITHERS, R. L., THOMSON, J. G. & BUTLER, B. D. (1992). *J. Solid State Chem.* In the press.
YAMAMOTO, A. & NAKAZAWA, H. (1982). *Acta Cryst.* A**38**, 79-86.

Acta Cryst. (1992). A**48**, 746-751

Polarized Dispersion, Glide-Rule-Forbidden Reflections and Phase Determination in Barium Bromate Monohydrate

BY DAVID H. TEMPLETON AND LIESELOTTE K. TEMPLETON

Department of Chemistry, University of California, Berkeley, CA 94720, *USA*

(*Received* 6 *December* 1991; *accepted* 16 *March* 1992)

Abstract

Reflections forbidden by a glide-plane rule are observed in diffraction experiments with a crystal of barium bromate monohydrate using linearly polarized synchrotron radiation with wavelength near the bromine *K*-absorption edge. Their intensities change with azimuth in agreement with equations derived using a tensor model of the anomalous scattering of the bromate ion and are consistent in scale with earlier measurements of that tensor in sodium bromate. The intensity of each forbidden $h0l$ reflection gives the magnitude and phase of the bromine part of the structure factor of the allowed $2h,0,2l$ reflection. The x and z coordinates of the Br atom determined from such data for 11 reflections are within 0.02 Å of those from two crystal structure determinations.

1. Introduction

Polarization-dependent absorption of X-rays (dichroism or pleochroism) has been observed in many materials now that synchrotron radiation provides polarized beams at the wavelengths near absorption edges where this dichroism is most significant (see review by Brouder, 1990). With it comes birefringence of the complex index of refraction, polarization anisotropy of the anomalous scattering terms and changes of intensities and polarization states of scattered rays (see, for example, Belyakov & Dmitrienko, 1989). One result is that some Bragg reflections that are forbidden by the ordinary space-group rules for screw axes and glide planes can be observed (Templeton & Templeton, 1980, 1985; Dmitrienko, 1983, 1984). These effects are new sources of information about the structures of crystals. The change of intensity of a Bragg reflection with azimuth can be used to determine phases of structure factors (Templeton & Templeton, 1991) in much the same way as the change with wavelength in the absence of birefringence (the MAD method). The azimuthal intensity variation of reflections forbidden by a screw-axis rule in sodium bromate, $00l$ with l odd, gave the phases for $0,0,2l$ reflections (Templeton & Templeton, 1987). The intensities of these forbidden reflections depend only on the structure of the anisotropic atoms and they can be used to determine that partial structure (Templeton & Templeton, 1986; Kirfel & Petcov, 1991). Here we report a study of reflections that are forbidden by a glide-plane rule and show how to get structure-factor phases from their intensities. The experiments were done at the Stanford Synchrotron Radiation Laboratory.

0108-7673/92/050746-06$06.00